



Regular Article

## A collective motion description of tubulin $\beta$ T7 loop dynamics

Sarbani Chattopadhyaya, Debamitra Chakravorty and Gautam Basu

Department of Biophysics, Bose Institute, VIIM, Kolkata 700054, India

Received July 1, 2019; accepted July 18, 2019

**Tubulin is a hetero-dimeric protein that polymerizes into microtubules and facilitates, among other things, eukaryotic cell division. Thus, any agent that interferes with tubulin polymerization is of therapeutic interest, vis-à-vis cancer. For example, colchicine is known to prevent tubulin polymerization by binding at the hetero-dimeric interface of  $\alpha\beta$ -tubulin. Crystal structures of tubulin bound to colchicine have shown that the dynamical conformation of a loop ( $\beta$ T7) plays an important role in colchicine binding. The  $\beta$ T7 loop dynamics also plays an important role in yielding curved versus straight  $\alpha\beta$ -tubulin dimers, only the latter being compatible with the microtubule assembly. Understanding the molecular mechanism of inhibition of microtubule assembly can lead to development of better therapeutic agents. In this work we were able to capture the  $\beta$ T7 loop flip by performing 200 ns molecular dynamics simulation of ligand-free  $\alpha\beta$ -tubulins. The loop flip could be described by only two independent collective vectors, obtained from principal component analysis. The first vector describes the flip while the second vector describes the trigger. The collective variables identified in this work is a natural reaction coordinate for functionally important tubulin dynamics, which allowed us to describe in detail the interaction network associated with the flip and the overall straight/curved conformational equilibrium.**

**Key words:** tubulin loop dynamics, colchicine binding site, collective motion,  $\beta$ T7 loop flip

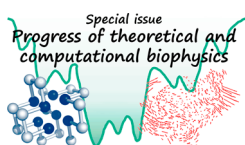
The essential eukaryotic protein tubulin is made up of two homologous chains ( $\alpha$  and  $\beta$ ) [1]. Hetero-dimeric tubulin can polymerize to form microtubules (Fig. 1A) which is an essential part of the machinery required for cell division. Microtubules undergo stochastic periods of growth and shrinkage known as dynamic instability [2,3]. Small molecules can bind tubulin (Fig. 1B) and affect microtubule dynamics or the tubulin/microtubule equilibrium [4]. Two kinds of conformations of tubulin are known from the atomistic crystal structures of GDP-bound tubulin. In one form, tubulin forms antiparallel protofilaments on two dimensional zinc sheets, stabilized by taxol [5]. It was reported that tubulin must adopt this conformation, known as 'straight', to be incorporated in the microtubule lattice [6,7]. The other conformation is known as the 'curved' conformation. This conformation has been reported from structure obtained from the crystal of " $\alpha\beta$ - $\alpha\beta$ " tubulin complexed with stathmin-like domain, either bound with with DAMA colchicine or without any ligand at the colchicine binding site [8]. The curved conformation is incompatible with microtubule lattice and is typically associated with free (unpolymerized) tubulin heterodimers [8].

Tubulin monomers ( $\alpha$  and  $\beta$ ) share ~40% sequence identity and high structural similarity. They can be decomposed into three domains [8]: (i) N-terminal nucleotide-binding

Corresponding author: Gautam Basu, Department of Biophysics, Bose Institute, P-1/12 CIT Scheme VIIM, Kolkata 700054, India.  
e-mail: [gautam@jcbose.ac.in](mailto:gautam@jcbose.ac.in)

### ◀ Significance ▶

Tubulin, an essential eukaryotic protein that plays an important role in cell division, is a target for anti cancer drugs. The binding of the anti-mitotic drug colchicine to tubulin is modulated by the conformational flip of a loop that also controls the polymerization of tubulin into microtubule. Flipped and un-flipped conformations of the loop are known but a detailed dynamic picture of the transition is poorly understood. Here we describe the flip by a reaction coordinate defined by two collective vectors—one captures the core flip and the other depicts the trigger to the flip.



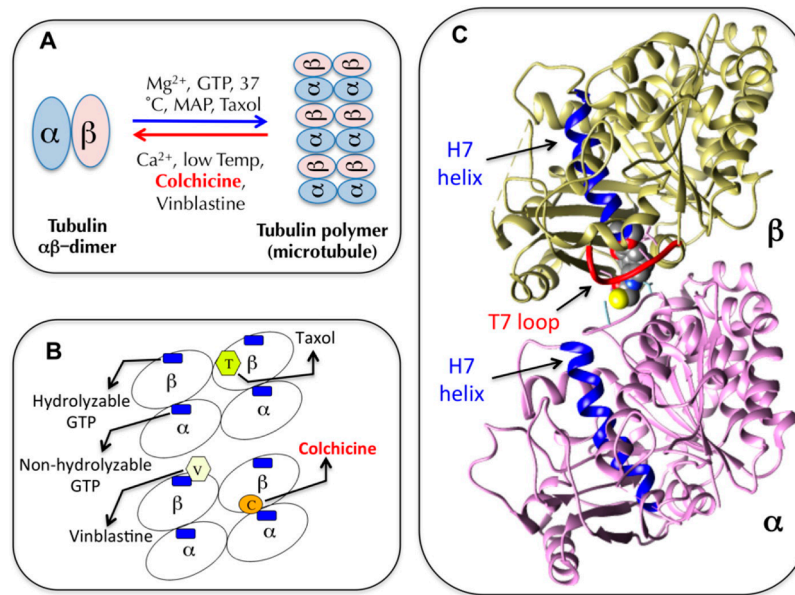


**Figure 1** (A) Tubulin  $\alpha\beta$ -dimer in equilibrium with microtubule. Different conditions (or molecules) that affect the equilibrium are summarized. (B) A schematic showing binding of small molecules (taxol, colchicine and vinblastine) with tubulin. The approximate binding sites of the hydrolyzable and non-hydrolyzable GTP molecules are also shown. (C) The X-ray crystal structure of tubulin  $\alpha\beta$ -dimer bound to colchicine (PDB ID: 1SA0). The  $\beta$ T7 loop, covering the bound colchicine molecule is shown in red. The H7 helices in the two monomers are shown in blue. The relative orientations of the two helices are different in the straight and curved conformations of the dimer.

domain: residues 1–206; (ii) Intermediate domain: residues 207–381; (iii) C-terminal: residues 382–440 [6]. The relative orientations of the three domains for both  $\alpha$  and  $\beta$  monomers are different in the straight and the curved conformations of tubulin [8]. The noticeable local differences between the curved and straight structures mainly comprise of conformational changes in loops located at the  $\alpha$ - $\beta$  intra-dimer longitudinal interfaces in protofilaments. It involves a movement of the  $\beta$ T7 loop and H8 helix [8] of the  $\beta$  subunit (see Fig. 1C for the locations of the  $\beta$ T7 loop). Multiple rotational and translational motions in the  $\alpha$ - and the  $\beta$ -subunits differentiate the straight and the curved conformations. One robust way of quantifying the straight/curved transition is to monitor the relative orientations of the H7 helices in the  $\alpha$ - and  $\beta$ -subunits [9] (see Fig. 1C for the locations of the H7 helices).

Crystal structures of tubulin bound to colchicine [8] revealed that colchicine binds to the  $\beta$ -tubulin at the intra-dimer interface to lock the  $\alpha$ - $\beta$  tubulin curved conformation. This in turn prevents it from adopting the straight conformation required for microtubule polymerization [8]. The major difference between the un-liganded curved tubulin and the colchicine-bound tubulin complex was found in the structure of  $\beta$ T7 loop [10]. The  $\beta$ T7 loop has three different conformations: (i) that in the straight tubulin molecule, (ii) that in the curved un-liganded molecule and (iii) that in the curved tubulin-colchicine complex [10]. The  $\beta$ T7 loop comprises of three highly conserved residues in both tubulin subunits (Gly-X-X-Asn-X-Asp). In the unliganded structure

the  $\beta$ T7 loop occupies the space of the colchicine binding site. The Asn249 $\beta$  residue appears in the space that is occupied by the ‘A’ ring of colchicine in tubulin-colchicine complex. The structural dynamics shows that when tubulin is approached by colchicine, the  $\beta$ T7 loop *flips* to make space for the incoming colchicine [10]. The  $\beta$ T7 loop is also involved in mediating longitudinal contacts with the neighboring molecule in microtubules [10].

Though the crystal structures provide critical information about ligand-bound and ligand-free structures, the molecular mechanism behind the dynamics connecting the ligand-bound and the ligand-free structures can only be obtained from atomistic simulations. Also, atomistic simulations allow one to filter out correlated motions. Therefore, although the dynamics of single residues like Asn249 $\beta$  are known to be important for the  $\beta$ T7 loop flip, we wanted to explore global changes in intra-protein signaling network that accompany the  $\beta$ T7 loop flip. The molecular simulations and analyses presented here provides a better understanding of straight/curved transitions of tubulin further unravelling the coordinated local interactions that allow or disallow colchicine binding.

## Materials and Methods

Three crystal structures of tubulin dimer were obtained from the protein data bank: (1) ligand-free “curved” animal tubulin dimer (PDB ID: 3HKB), (2) “straight” animal tubulin dimer (PDB ID: 1JFF), (3) colchicine-bound “curved” ani-

mal tubulin dimer (PDB ID: 1SA0). Only the first structure was used as the starting conformation for MD simulations. The other two were used for reference purposes. The missing residues/atoms were homology modeled. All simulations were performed with the OPLS/AA forcefield [11]. The parameters for GTP and GDP, not available in the OPLS/AA force field, were used from the archive of AMBER parameter database [12] since the OPLS/AA parameters are functionally similar to Amber force field parameters [13]. Modifications were made to the hydrogen database `ffoplsaa.hdb` and residue type database `ffoplsaa.rtp` for OPLS/AA forcefield in Gromacs 4.0.7 [14] package to include the information about the atoms (including hydrogen), bonds and improper dihedrals of the two molecules.

Gromacs version 4.0.7 was used to perform the simulations. Two separate 200 ns simulations with different velocity seeds were performed on the colchicine-free curved animal tubulin dimer (PDB ID: 3HKB) structure. The OPLS/AA force field was used with SPC water model [15]. The hydrogen bonds were constrained using the LINCS algorithm [16]. The integration time step used was 1 fs. The neighbor list update was done every 10 steps. Berendsen coupling method [17] was used to maintain the temperature at 298 K and pressure at 1 atm. An initial energy minimization using the Steepest descent method was done before the production run. The non-bonded electrostatic interactions were calculated using the Particle Mesh Ewald method [18]. The trajectory was analyzed using in-house FORTRAN codes. Principal component analysis was also performed using in-house FORTRAN codes.

The curvature of tubulin dimer over the simulation time was calculated. The angle used to determine the curvature is defined by the intra-dimer rotation angle between the planes of each of the snapshot (obtained from simulations) with respect to that of the straight tubulin structure (PDB ID: 1JFF) [9], after structurally superimposing each structure onto the straight tubulin by the  $\alpha$ -subunit H7 helices [9]. All-atom superposition was done. The angle was calculated between the planes to the  $\alpha$ - and  $\beta$ -subunit H7 helices. Residues 224–242 and 224–243 of the  $\alpha$ - and  $\beta$ -subunits respectively were used to define respective H7 helices for the straight tubulin structure (PDB ID: 1JFF). Residues 224–244 of the  $\alpha$ -subunit and 224–242 of  $\beta$ -subunit are used to define

H7 helices of (curved) animal tubulin (PDB ID: 3HKB). The superimposition, the plane definition and the angles were calculated using CHIMERA [19].

## Results and Discussion

The colchicine-binding site at the  $\alpha\beta$  intra-dimer interface comprises the  $\beta$ H7,  $\beta$ H8 helices, the  $\beta$ T7 loop and the  $\beta$ S7–S9 sheets—all parts of the  $\beta$ -intermediate domain. Colchicine also interacts with the  $\alpha$ T5 loop. The local structural differences between the straight and the curved tubulin conformations at the intra-dimer  $\alpha\beta$  interface comprise movement of the  $\beta$ T7 loop and  $\beta$ H8 helix, and in the conformations of the  $\alpha$ T5 and  $\beta$ H6–H7 loops, which lie close to the colchicine-binding site. The aim of the present work is to provide insights into the interaction network of residues from these secondary structural elements at the  $\alpha\beta$  intra-dimer interface in the free (colchicine-unbound) tubulin heterodimer. The dynamics of  $\beta$ T7 loop, present at the  $\alpha\beta$  intra-dimer interface, is known to modulate both colchicine binding and the ability of tubulin to be accommodated in the microtubule. Therefore the focus was on the movement of this loop.

### Observation of $\beta$ T7 loop flip

Two separate 200 ns simulations, cTub1 and cTub2, with different velocity seeds, were performed on the unliganded curved wild type tubulin (PDB ID: 3HKB). As shown in Figure 2A–B, the time evolution of RMSD (C $\alpha$  only) revealed large variation (upto 4.5 Å in first simulation and 3.0 Å in the second simulation). However, since the system is a dimeric protein, the RMSD includes both intra as well as intermolecular deviations. To focus only on the intramolecular deviation, we separately calculated the RMSD for the  $\alpha$ - and the  $\beta$ -chains in each of the simulations. As shown in Figure 2A–B, the subunit RMSD values showed a plateau around 2.0 Å. Since the focus of this work is on the dynamics of the  $\beta$ T7 loop, we closely analyzed the  $\beta$ T7 loop conformations in the two simulations at atomistic details. It was found that the  $\beta$ T7 loop flipped in around 100 ns in the first simulation but it remained in the un-flipped conformation for the entire 200 ns in second simulation.

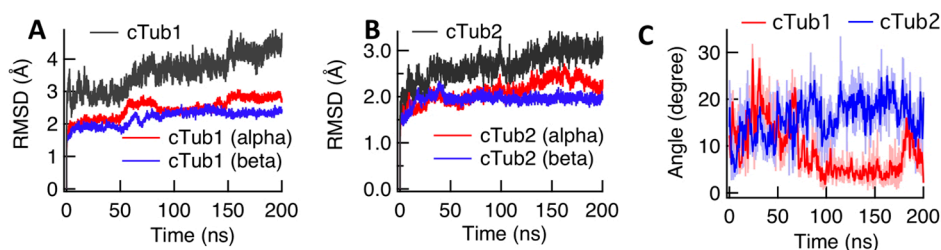


**Figure 2** Time evolution of backbone RMSD (C $\alpha$  atoms only) of: (A) cTUB1 and (B) cTub2 simulations. (C) The time evolution of the ‘intra-dimer’ angle (with respect to straight animal tubulin) of tubulin heterodimer cTUB1 (red) cTub2 (blue).

### Time evolution of the curvature along the trajectories

Since the flipping of the  $\beta$ T7 loop is associated with tubulin curvature [9], the curvature of the tubulin structure over the simulation time was investigated. Following the method of Peng, L. X., *et al.* [9], the intra-dimer angle, symbolizing the angle of curvature, was calculated by superimposing the trajectory snapshots, every 20 ps, on the straight structure (superimposing the  $\alpha$ H7 helices) and calculating the angle between the planes defined by the  $\alpha$ H7 and  $\beta$ H7 helices. The intra-dimer angle between the crystal structure of the curved tubulin heterodimer ' $\alpha$ 1 $\beta$ 1' (PDB ID: 3HKB), which is the initial structure for the current simulations and the reference straight structure (PDB ID: 1JFF) was  $8.67^\circ$ . This angle was calculated to be  $7.77 \pm 1.8^\circ$  by Peng, L. X., *et al.* [9]. The time evolution of the animal wild type curved tubulin structure show different trends for the two simulations. (Fig. 2C). The first simulation had shown the  $\beta$ T7 loop flip to occur at around  $\sim 100$  ns. It is seen that the intra-dimer angle for the first simulation during the period  $\sim 100$  ns to

$\sim 180$  ns was close to  $0^\circ$ . Thus the  $\beta$ T7 loop flip accompanied by the structural rearrangement of the neighboring secondary structure elements led to the adoption of conformation by the heterodimer which was more alike the straight conformation. However such lowering of the intra-dimer angle was not observed for the second simulation, which did not witness the  $\beta$ T7 loop flip.

### $\beta$ T7 loop flip captured in Ca only PCA

To better understand the nature of structural changes in the trajectory, PCA was performed on both the trajectories. As shown in Figure 3A–B, when projected along the PC2–PC1 plane, several clusters were observed. However, instead of analysing the clusters or the motion along the PC axes, we performed a similar PCA only on the  $\beta$ -subunits of both the simulations, since the focus of this work is on the  $\beta$ T7 loop, present in the  $\beta$ -chain.

As shown in Figure 3C–D, PCA on the  $\beta$ -subunit also revealed a number of clusters when the trajectories were

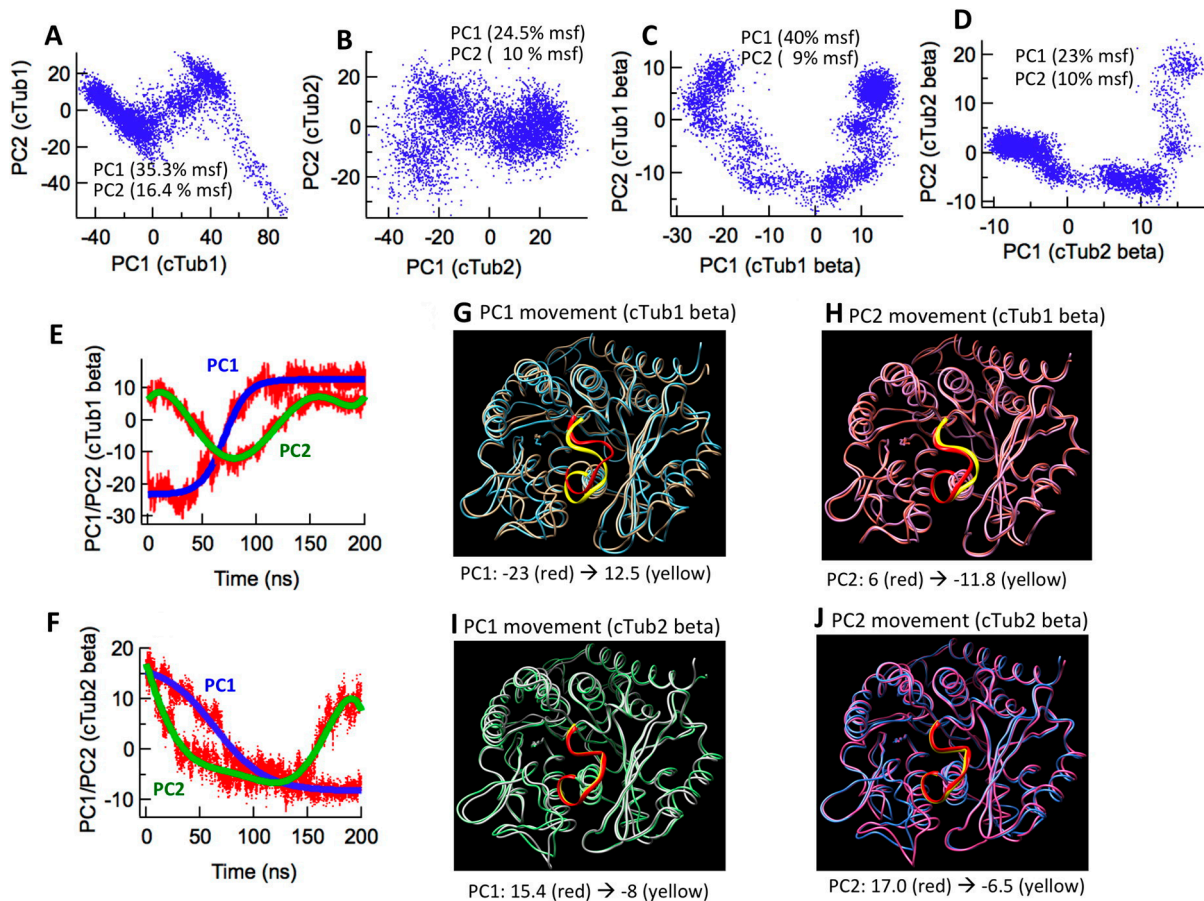


**Figure 3** Projection of trajectories of  $\alpha\beta$ -heterodimeric tubulin on the first two PC axes (Ca atoms only) for: (A) cTUB1 and (B) cTub2 simulations. Projection of trajectories of  $\beta$ -tubulin on the first two PC axes (Ca atoms only) for: (C) cTUB1 and (D) cTub2 simulations. Time evolution of  $\beta$ -tubulin PC1 and PC2 axes (Ca atoms only) for: (E) cTub1 and (F) cTub2 simulations. Conformational change of  $\beta$ -tubulin along: (G) PC1 and (H) PC2 axes corresponding to cTUB1 simulation. Conformational change in of  $\beta$ -tubulin along: (I) PC1 and (J) PC2 axes corresponding to cTUB2 simulation. Panels (G)–(J) contain two superimposed structures, corresponding to two PC values, as indicated below the panels. The  $\beta$ T7 loop is highlighted in red (start value) and yellow (end value).

projected on the PC1-PC2 axes. The percent contribution of PC1 and PC2 towards the total mean square fluctuation (msf), as reflected in the eigen values, were higher in cTub1 (PC1: 40% and PC2: 9%) than in cTub2 (PC1: 23% and PC2: 10%). The time evolution of PC1 and PC2 axes for both the simulations are shown in Figure 3E-F. For both cases, PC1 showed a shift along the time axis, from -20 to 10 in cTub1 and from 15 to -8 in cTub2.

To better understand the kind of backbone changes associated with the PC1 axes in the two simulations,  $\beta$ -tubulin structures were generated corresponding to the two extreme values of PC1 in both cases. The end point structures are shown superposed in Figure 3G-J with a special emphasis on the state of the  $\beta$ T7 loops (colored red for the initial PC value and yellow for the final value). This showed a stark difference between the two simulations. In the first simulation (cTub1), the  $\beta$ T7 loop undergoes a large conformational change along the PC1 axis (Fig. 3G). However, there is almost no effect on the conformation of the  $\beta$ T7 loop as  $\beta$ -tubulin changes its backbone structure along PC1 in the second simulation (cTub2; Fig. 3I). When  $\beta$ -tubulin structures were generated along PC2, very similar effect was seen—in cTub1 simulation (Fig. 3H), the  $\beta$ T7 loop conformation changes but movement along PC2 does not affect the  $\beta$ T7 loop structure in cTub2 simulation (Fig. 3J). In other words, the  $\beta$ T7 loop flips in the first simulation (cTub1) and the flip is captured very well by the first and the second PC vectors. On the other hand the second simulation (cTub2) shown no such flip.

### $\beta$ T7 loop flip as seen in all atom PCA

To probe the  $\beta$ T7 loop flip, observed in the first simulation, at atomic detail, we performed further PCA analysis on cTub1, considering only residues (all atoms) within 5 Å of the core  $\beta$ T7 loop residues. Results are shown in Figure 4A (projection on the PC2-PC1 plane) and in Figure 4B (time evolution of PC1 and PC2). Interestingly, the PC2-PC1 scatter plot and the time evolution of PC1/PC2 from the  $C\alpha$ -only  $\beta$ -tubulin trajectory (Figs. 3C and 3E) matches very well with that performed on the subset of atoms (all) close to the  $\beta$ T7 loop (Fig. 4A-B). For example, Pearson's correlation coefficient between PC1 of Figure 3E and PC1 of 4A was -0.94 while that between PC2 of Figure 3E and PC2 of 4A was 0.76. This indicates that the conformational change observed around the  $\beta$ T7 loop is the dominant conformational change observed in the PCA of the whole protein.

The first PC vector, PC1 representing 45% msf, shows a clear two state transition except for some conformational changes during the first 10 ns. The second PC vector, PC2, representing 8.5% of msf, changes with PC1 in a correlated fashion until the midpoint of transition and then changes in an anti-correlated fashion. Analysis of structural changes associated with PC1 (Fig. 5) showed that indeed, the transition associated with PC1 is the  $\beta$ T7 loop flip.

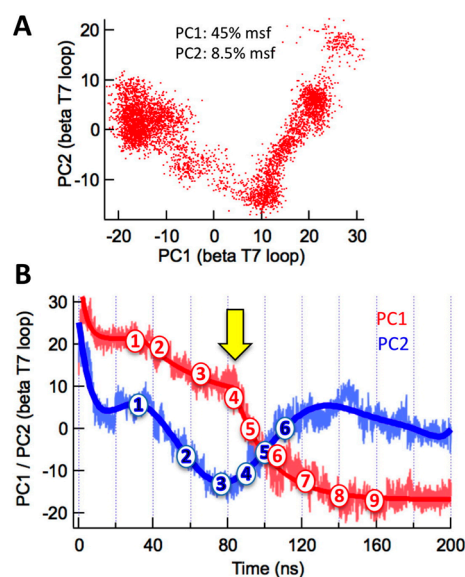


**Figure 4** (A) Projection of PCA of  $\beta$ T7 loop residues (cTUB1) along PC1 and PC2 axes. (B) Time evolution of PC1 and PC2 from PCA of  $\beta$ T7 loop (cTUB1) simulation. The numbers (1-6 for PC2 and 1-9 for PC1) refer to points for which the H-bond networks are shown in Figures 5, 6 and 7.

### PC1: a collective description of $\beta$ T7 loop flip

Nine time points, annotated on PC1 line in Figure 4B, are shown in Figure 5. Specifically, we focus on the H-bonding network (see Table 1). Several H-bonds are maintained throughout the transition (*Sl. No. 17–22 Table 1*). Some start forming as the transition proceeds but are not sustained throughout—they get disrupted soon, definitely after the transition midpoint (*Sl. No. 1–9 Table 1*). Some H-bonds start forming after the transition has proceeded a little; they are sustained until the end (*Sl. No. 12–15 Table 1*). And there are some that form only around the transition midpoint, disappearing as the transition ends (*Sl. No. 10–11 Table 1*).

Analysis of Table 1 and Figure 5 clearly shows that the hall mark of the transition is reflected in interactions of ASN 249.B side chain. At the beginning, the side chain ND2 atom of ASN 249.B forms a H-bond with the backbone oxygen atom of THR 179.A. This inter-chain interaction gets disrupted as the  $\beta$ T7 loop flips, resulting in a new inter-chain interaction: the side chain ND2 atom of ASN 249.B forms a H-bond with the side chain OE2 oxygen atom of GLU 71A. Concomitantly, the H-bond network changes for many pairs as noted in Table 1 (and Fig. 5). For example, after the flip, OE2 oxygen atom of GLU 71A forms a bifurcated H-bond with NZ atom of LYS 254.B, and the OE1 oxygen atom of GLU 71A forms a H-bond with NH2 atom of ARG 2.B. Before the flip, the backbone oxygen atom of THR 179.A participated in a bifurcated H-bond with the ND2 atom of ASN 258.B, which gets disrupted with the flip as does a side chain side chain H-bond involving THR 179.A (between OG1 of THR 179.A and OD1 atom of ASN 258.B). The

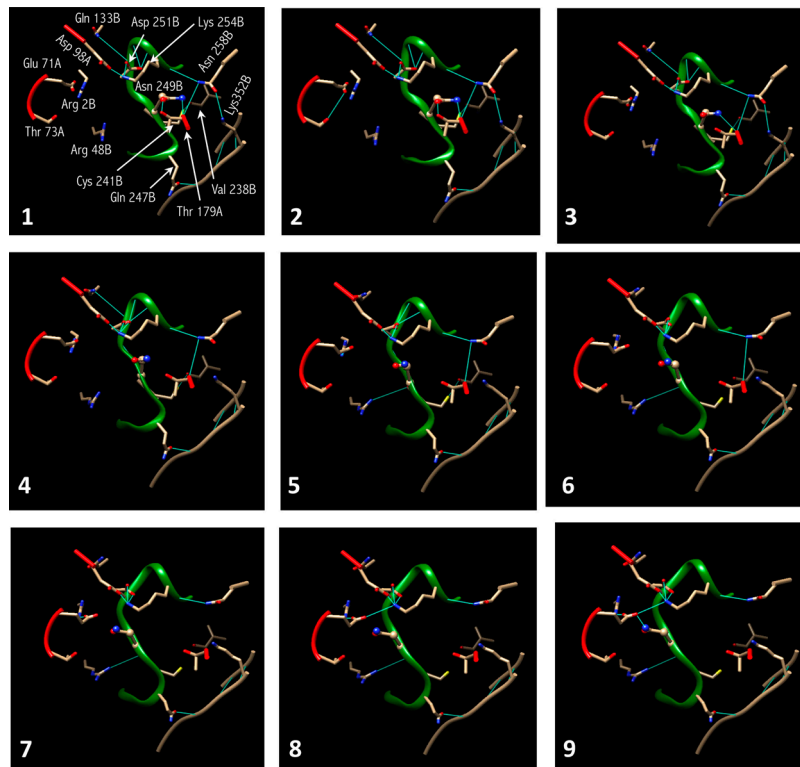


**Figure 5** Hydrogen bonding network dynamics of the  $\beta$ T7 loop residues (along PC1 axis for cTub1 simulation). The nine frames are marked in Figure 4B and the atomic coordinates are available in Supplementary Materials S1 and S2. This figure should be read with Table 1 and Figure 6.

network of H-bond that change in a collective fashion is depicted schematically in Figure 6. The transition (along PC1) is also summarized in the movie PC1. Like the ND2 atom of ASN 249.B, the OD2 atom of ASP 251.B also changes H-bonding partner before and after the flip. Before the flip the OD2 atom is H-bonded to the NZ atom of LYS 254.B but this gets disrupted and a bifurcated H-bond appears after the flip (H-bonds with N atoms of ARG 253.B and LYS 254.B). To achieve this the side chain of ASP 251.B flips ( $\chi^2$  flips by  $\sim 180^\circ$ ). Most of the changes described here are polar in nature (H-bonds). This is probably because the loop is dominated by polar side chains. However, non-polar interactions also showed some change as the loop flipped. For example, packing of side chains of ALA 316.B and LYS 352.B showed considerable difference upon  $\beta$ T7 loop flip. Motion depicting the movement of the  $\beta$ T7 loop and its neighbors along the PC1 axis (nine points shown in Fig. 4) is summarized in the Supplementary movie S1.avi.

#### PC2: a collective description of “trigger” to $\beta$ T7 loop flip

Similar to the case of PC1, the H-bond network dynamics also changes along PC2, as the  $\beta$ T7 loop flips. This has been captured in six frames (see Fig. 4B and Fig. 7). As was the case with PC1 axis, several H-bonds remain stable through out the loop flip transition along PC2 axis as well (*Sl. No. 10–19 Table 2*). Some H-bonds are seen only at the

beginning and at the end of the transition (*Sl. No. 1–4 Table 2*), while some are observed only at the midpoint (*Sl. No. 7–9 Table 2*).

Unlike PC1, which changes in a sigmoid fashion from +20 to -20, with a midpoint around 80 ns, major variation of PC2 is best represented by an inverted gaussian function. When changes in PC1 reaches the half value at  $\sim 80$  ns, changes in PC2 reaches its maximum negative value, after which it recedes to its original value. Since PC1 and PC2 are orthogonal, meaning motions along the two axes are decoupled, it seems that PC2 is the trigger for the PC1 transition. A careful look at Figure 4B (see yellow arrow) shows that a sharp jump in PC2 is triggered by PC2 – only after PC2 crosses its maximum (negative) value of  $\sim -10$ , PC1 shows a sharp transition. If indeed PC2 is the trigger for the PC1 transition ( $\beta$ T7 loop flip), specific interactions associated with this trigger should be reflected in Figure 6 (and Table 2) and Figure 7.

Two residues, LYS 352.B and ASP 251.B play a crucial role in stabilizing the so called transition state that connects the unflipped and flipped conformations of the  $\beta$ T7 loop (frames 3 and 4 of Table 2; see Fig. 6). We had earlier seen how the side chain of ASP 251.B undergoes a flip when the  $\beta$ T7 loop flips. In frames 3 and 4, the side chain flip is half-way complete and the “intermediary” conformation is stabilized by a H-bond between the side chain OD1 atom of ASP

**Table 1** Hydrogen bond network during  $\beta$ T7 loop flip (along PC1)

Sl. No.	Donor	Acceptor	Distance ( $\text{\AA}$ )* (first frame)	H-bond (per frame)# 1-2-3-4-5-6-7-8-9
1	THR 179.A OG1	ASN 249.B OD1	3.14	1-1-0-0-0-0-0-0-0
2	THR 73.A OG1	GLU 71.A OE1	3.51	0-1-0-0-0-0-0-0-0
3	ASN 249.B ND2	THR 179.A O	2.37	1-1-1-0-0-0-0-0-0
4	LYS 352.B NZ	ASN 258.B OD1	3.28	1-1-1-0-0-0-0-0-0
5	GLN 133.B NE2	ASP 251.B O	3.54	1-1-1-1-0-0-0-0-0
6	CYS 241.B SG	VAL 238.B O	3.37	1-1-1-1-1-0-0-0-0
7	ARG 253.B N	ASP 251.B OD2	2.97	1-1-1-1-1-0-0-0-0
8	LYS 254.B N	ASP 251.B OD2	2.78	1-1-1-1-1-0-0-0-0
9	ASN 258.B ND2	THR 179.A O	2.85	1-1-1-1-1-1-0-0-0
10	GLN 133.B NE2	ASP 251.B O	3.27	0-0-0-1-0-0-0-0-0
11	ASP 251.B N	ASN 249.B O	2.94	0-0-0-1-1-1-0-0-0
12	LYS 254.B NZ	ASP 251.B OD2	3.41	0-0-0-1-1-1-1-1-1
13	ARG 2.B NH2	GLU 71.A OE1	3.34	0-0-0-0-1-1-1-1-1
14	ARG 48.B NH1	LEU 242.B O	3.50	0-0-0-0-1-1-1-1-1
15	LYS 254.B NZ	GLU 71.A OE2	3.46	0-0-0-0-0-0-0-0-1
16	ASN 249.B ND2	GLU 71.A OE2	3.04	0-0-0-0-0-0-0-0-1
17	LYS 254.B NZ	ASP 98.A OD2	2.72	1-1-1-1-1-1-1-1-1
18	LYS 254.B NZ	ASP 251.B OD1	2.67	1-1-1-1-1-1-1-1-1
19	ASN 258.B ND2	LYS 254.B O	2.96	1-1-1-1-1-1-1-1-1
20	ALA 317.B N	LYS 352.B O	3.13	1-1-1-1-1-1-1-1-1
21	ALA 354.B N	ALA 317.B O	3.10	1-1-1-1-1-1-1-1-1
22	VAL 355.B N	GLN 247.B OE1	3.35	1-1-1-1-1-1-1-1-1

\* The distance is between the donor and the acceptor atom in the first frame the H-bond was observed. # The nine frames are numbered 1 if a H-bond was observed and 0 if there were no H-bonds.

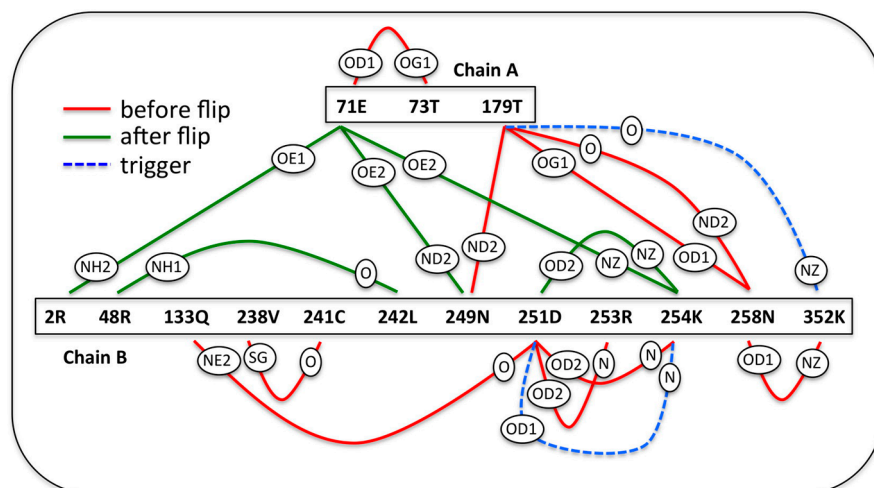


**Figure 6** A schematic depicting the status of key H-bonds involving the  $\beta$ T7 loop and its neighbors (within  $5 \text{\AA}$ ) before (red) and after (green) the loop flips (according to PC1). The H-bonds shown by the broken blue lines trigger the flip (according to PC2). This figure should be read with Tables 1 and 2 and Figures 5 and 7.

251.B H-bonded to the backbone N atom of LYS 254.B. The OD1 atom of ASP 251.B is not H-bonded before or after the flip but only contributes to the intermediary conformation. The other residue that plays a critical role in stabilizing the intermediary conformation is LYS 352.B. Before the flip, the side chain NZ atom of LYS 352.B forms a H-bond with the

OD1 atom of ASN 258.B. This gets disrupted as a result of the flip. However, not before the NZ atom of LYS 352.B plays an important role to transiently stabilize the intermediary conformation by forming a H-bond with the backbone oxygen atom THR 179.A. Interestingly, the backbone oxygen atom THR 179.A forms a H-bond in the unflipped state

**Table 2** Hydrogen bond network during  $\beta$ T7 loop flip (along PC2)

Sl. No.	Donor	Acceptor	Distance ( $\text{\AA}$ )* (first frame)	H-bond (per frame)# 1-2-3-4-5-6
1	ARG 2.B NH1	GLU 71.A OE1	3.496	1-0-0-0-0-0
2	ARG 2.B NH2	GLU 71.A OE1	3.083	0-0-0-0-0-1
3	CYS 241.B SG	VAL 238.B O	3.689	1-0-0-0-0-1
4	ALA 354.B N	ALA 317.B O	2.997	1-0-0-0-1-1
5	GLN 133.B NE2	ASP 251.B O	3.570	0-1-0-0-1-0
6	LYS 254.B N	ASP 251.B OD2	3.308	0-1-1-1-1-1
7	LYS 352.B NZ	THR 179.A O	3.546	0-1-1-1-0-0
8	LYS 254.B N	ASP 251.B OD1	3.456	0-0-1-1-0-0
9	LYS 352.B NZ	ASN 258.B OD1	3.325	0-0-1-0-0-0
10	ASP 251.B N	ASN 249.B O	3.029	1-1-1-1-1-1
11	ARG 251.B N	ASP 251.B OD2	3.453	1-1-1-1-1-1
12	LYS 254.B NZ	ASP 98.A OD2	2.627	1-1-1-1-1-1
13	LYS 254.B NZ	ASP 251.B OD1	2.893	1-1-1-1-1-1
14	LYS 252.B NZ	ASP 251.B OD2	3.078	1-1-1-1-1-1
15	ASN 258.B ND2	THR 179.A O	3.475	1-1-1-1-1-1
16	ASN 258.B ND2	LYS 254.B O	2.837	1-1-1-1-1-1
17	ALA 317.B N	LYS 352.B O	3.032	1-1-1-1-1-1
18	VAL 355.B N	GLN 247.B OE1	3.496	1-1-1-1-1-1
19	ARG 48.B NH1	LEU 242.B O	3.523	1-1-1-1-1-1

\* The distance is between the donor and the acceptor atom in the first frame the H-bond was observed. # The nine frames are numbered 1 if a H-bond was observed and 0 if there were no H-bonds.

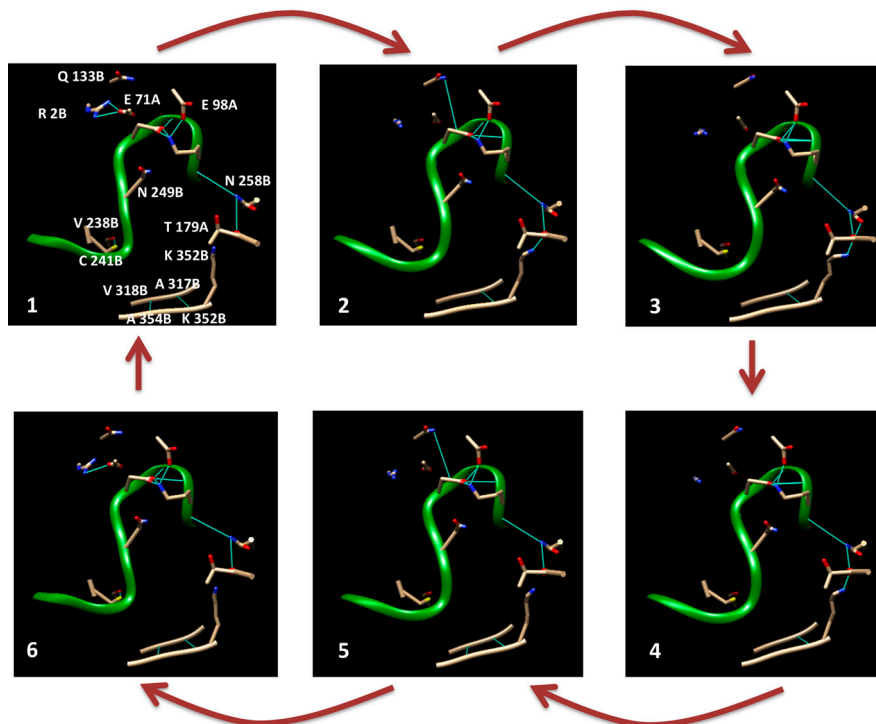


**Figure 7** Hydrogen bonding network dynamics of the  $\beta$ T7 loop residues (along PC2 axis for cTub1 simulation). The six frames are marked in Figure 4B and the atomic coordinates are available in Supplementary Materials S1 and S2. This figure should be read with Table 2 and Figure 6.

which gets disrupted upon flipping. But just like the NZ atom of LYS 352.B, the oxygen atoms plays an important role in stabilizing the intermediary conformation. Motion depicting the movement of the  $\beta$ T7 loop and its neighbors along the PC2 axis (six points shown in Fig. 4) is summarized in the Supplementary movie S2.avi.

Therefore, while PC1 allowed us to map the detailed H-bond network dynamics during the  $\beta$ T7 loop flip, PC2 allowed us to point out interactions that trigger this loop flip.

## Conclusion

By suitable analysis (PCA) of the 200 ns tubulin trajectory, where a  $\beta$ T7 loop flip was observed, we could identify the essential motion (as reflected in PC1) associated with the conformational change. This allowed us to probe the dynamics of hydrogen bonding network that changes as the loop flips. Not all motion was captured by PC1. PC2, which captured about 8% of mean square fluctuations, showed a very interesting trend; it changed as PC1 changed, but started to recede back once PC1 had moved halfway through the total move associated with the flip. The motion and interactions along PC2 was proposed as the trigger for the ring flip. Specifically we found two key interactions for the flip to occur (as if these were “stabilizing” the “transition state”): (i) the side chain NZ atom of Lys 352.B needs to form a H-bond with the backbone O atom of THR 179.A and (ii) the backbone N atom of Lys 254.B needs to form a H-bond with the side chain oxygen atom of Asp 251.B. There could be more interactions that play a key role, either non H-bond type or beyond the 5 Å radius around the  $\beta$ -T7 loop, as considered here. Also, water molecules may also be involved as was shown in a recent molecular dynamics simulation study on tubulin [20]. These details can only be revealed in a more exhaustive work. In previous studies from this lab we had shown how subtleties in tubulin sequence can affect colchicine-sensitivity [21] or paclitaxel-sensitivity [22] across eukaryotes. This work demonstrates beautifully how a collective description of a conformational change associated with  $\beta$ T7 loop flip in tubulin is triggered by another collective mode.

## Acknowledgement

G. B. likes to acknowledge B. Bhattacharyya for stimulating discussions. S. C. and D. C. acknowledge financial support from ICMR and DST respectively.

## Conflict of Interest

S. C., D. C. and G. B. declare that they have no conflict of interest.

## Author Contribution

G. B. and S. C. conceived the work. S. C. and D. C. performed the MD simulations. S. C., D. C. and G. B. analyzed the data and wrote the manuscript.

## References

- [1] Tuszynski, J. A., Carpenter, E. J., Huzil, J. T., Malinski, W., Luchko, T. & Luduena, R. F. The evolution of the structure of tubulin and its potential consequences for the role and function of microtubules in cells and embryos. *Int. J. Dev. Biol.* **50**, 341–358 (2006).
- [2] Margolis, R. L. & Wilson, L. Opposite end assembly and disassembly of microtubules at steady state in vitro. *Cell* **13**, 1–8 (1978).
- [3] Mitchison, T. & Kirschner, M. Dynamic instability of microtubule growth. *Nature* **312**, 237–242 (1984).
- [4] Stanton, R. A., Gernert, K. M., Nettles, J. H. & Aneja, R. Drugs that target dynamic microtubules: a new molecular perspective. *Med. Res. Rev.* **31**, 443–481 (2011).
- [5] Xiao, H., Verdier-Pinard, P., Fernandez-Fuentes, N., Burd, B., Angeletti, R., Fiser, A., *et al.* Insights into the mechanism of microtubule stabilization by Taxol. *Proc. Natl. Acad. Sci. USA* **103**, 10166–10173 (2006).
- [6] Nogales, E., Wolf, S. G. & Downing, K. H. Structure of the alpha beta tubulin dimer by electron crystallography. *Nature* **391**, 199–203 (1998).
- [7] Löwe, J., Li, H., Downing, K. H. & Nogales, E. Refined structure of  $\alpha\beta$ -tubulin at 3.5 Å resolution. *J. Mol. Biol.* **313**, 1045–1057 (2001).
- [8] Ravelli, R. B. G., Gigant, B., Curmi, P. A., Jourdain, I., Lachkar, S., Sobel, A., *et al.* Insight into tubulin regulation from a complex with colchicine and a stathmin-like domain. *Nature* **428**, 198–202 (2004).
- [9] Peng, L. X., Hsu, M. T., Bonomi, M., Agard, D. A. & Jacobson, M. P. The Free Energy Profile of Tubulin Straight-Bent Conformational Changes, with Implications for Microtubule Assembly and Drug Discovery. *PLoS Comput. Biol.* **10**, e1003464 (2014).
- [10] Dorléans, A., Gigant, B., Ravelli, R. B. G., Mailliet, P., Mikol, V. & Knossow, M. Variations in the colchicine-binding domain provide insight into the structural switch of tubulin. *Proc. Natl. Acad. Sci. USA* **106**, 13775–13779 (2009).
- [11] Jorgensen, W. L. & Tirado-Rives, J. The OPLS [optimized potentials for liquid simulations] potential functions for proteins, energy minimizations for crystals of cyclic peptides and crambin. *J. Am. Chem. Soc.* **110**, 1657–1666 (1988).
- [12] Meagher, K. L., Redman, L. T. & Carlson, H. A. Development of polyphosphate parameters for use with the AMBER force field. *J. Comput. Chem.* **24**, 1016–1025 (2003).
- [13] Case, D. A., Cheatham, T. E., Darden, T., Gohlke, H., Luo, R., Merz, K. M., *et al.* The Amber biomolecular simulation programs. *J. Comput. Chem.* **26**, 1668–1688 (2005).
- [14] Van Der Spoel, D., Lindahl, E., Hess, B., Groenhof, G., Mark, A. E. & Berendsen, H. J. C. GROMACS: fast, flexible, and free. *J. Comput. Chem.* **26**, 1701–1718 (2005).
- [15] Berendsen, H. J. C., Postma, J. P. M., van Gunsteren, W. F. & Hermans, J. Interaction Models for Water in Relation to Protein Hydration, in *Intermolecular Forces*, (Pullman, B., ed.) pp. 331–342 (Springer, Netherlands, 1981).
- [16] Hess, B., Bekker, H., Berendsen, H. J. C. & Fraaije, J. G. E. M. LINCS: A linear constraint solver for molecular simulations. *J. Comput. Chem.* **18**, 1463–1472 (1997).
- [17] Berendsen, H. J. C., Postma, J. P. M., van Gunsteren, W. F.,

- DiNola, A. & Haak, J. R. Molecular dynamics with coupling to an external bath. *J. Chem. Phys.* **81**, 3684–3690 (1984).
- [18] Darden, T., York, D. & Pedersen, L. Particle mesh Ewald: An  $N$ -log( $N$ ) method for Ewald sums in large systems. *J. Chem. Phys.* **98**, 10089–10092 (1993).
- [19] Pettersen, E. F., Goddard, T. D., Huang, C. C., Couch, G. S., Greenblatt, D. M., Meng, E. C., *et al.* UCSF Chimera—a visualization system for exploratory research and analysis. *J. Comput. Chem.* **25**, 1605–1612 (2004).
- [20] Majumdar, S., Basu, D. & Ghosh Dastidar, S. Conformational states of E7010 is complemented by microclusters of water inside the  $\alpha,\beta$ -tubulin Core. *J. Chem. Inf. Model.* **59**, 2274–2286 (2019).
- [21] Banerjee, M., Roy, D., Bhattacharyya, B. & Basu, G. Differential colchicine-binding across eukaryotic families: the role of highly conserved Pro268 $\beta$  and Ala248 $\beta$  residues in animal tubulin. *FEBS Lett.* **581**, 5019–5023 (2007).
- [22] Das, L., Bhattacharyya, B. & Basu, G. Rationalization of paclitaxel insensitivity of yeast  $\beta$ -tubulin and human  $\beta$ III-tubulin isotype using principal component analysis. *BMC Res. Notes* **5**, 395 (2012).

---

This article is licensed under the Creative Commons Attribution-NonCommercial-ShareAlike 4.0 International License. To view a copy of this license, visit <https://creativecommons.org/licenses/by-nc-sa/4.0/>.

